

Chemical Science

Accepted Manuscript

This article can be cited before page numbers have been issued, to do this please use: J. Li, F. Wang, X. He, G. Huang, Z. Rong and X. Li, *Chem. Sci.*, 2026, DOI: 10.1039/D5SC08914J.



This is an Accepted Manuscript, which has been through the Royal Society of Chemistry peer review process and has been accepted for publication.

Accepted Manuscripts are published online shortly after acceptance, before technical editing, formatting and proof reading. Using this free service, authors can make their results available to the community, in citable form, before we publish the edited article. We will replace this Accepted Manuscript with the edited and formatted Advance Article as soon as it is available.

You can find more information about Accepted Manuscripts in the [Information for Authors](#).

Please note that technical editing may introduce minor changes to the text and/or graphics, which may alter content. The journal's standard [Terms & Conditions](#) and the [Ethical guidelines](#) still apply. In no event shall the Royal Society of Chemistry be held responsible for any errors or omissions in this Accepted Manuscript or any consequences arising from the use of any information it contains.

Rhodium-Catalyzed Atroposelective C-H Fluoroallylation of Heteroarenes with *gem*-Difluorocyclopropanes

Junwei Li,^a Fen Wang,^{a*} Xian He,^b Genping Huang,^{b,d*} Zi-Qiang Rong,^c Xingwei Li^{a*}

Received 00th January 20xx,
Accepted 00th January 20xx

DOI: 10.1039/x0xx00000x

Atroposelective C–H bond allylation represents an efficient and sustainable strategy toward construction of axially chiral functionalized biaryls. Yet existing systems are limited in reaction patterns using olefins and allyl ethers/esters. The lack of synthetic methods is ascribed to limited mechanistic pathways underlying such transformations. Reported herein is Rh(I)-catalyzed stereoconvergent axially chiral C–H fluoroallylation of non-electron-rich arenes using racemic *gem*-difluorocyclopropanes as bifunctional allyl precursors, which provides biaryls integrating allyl moiety and a fluorine atom. Mechanistic studies reveal a Rh(I)/Rh(III) oxidative addition–reductive elimination cycle involving C–H activation, β -F elimination, and rapid epimerization of the chiral axis, enabling selective reductive elimination to afford the axially chiral biaryl with high regio- and enantioselectivity. A representative product exhibits circularly polarized luminescence (CPL), highlighting the potential for high-performance chiral optoelectronic applications.

Introduction

Axially chiral biaryls have emerged as privileged molecular scaffolds owing to their pivotal roles in asymmetric catalysis,¹ drug discovery,² and functional materials.³ Consequently, the efficient and precise construction of axial stereogenicity has long been a central objective in asymmetric synthesis.⁴ In recent years, atroposelective C–H functionalization of arenes has become a highly efficient and atom-economical strategy for building axially chiral architectures,⁵ offering a sustainable and more atom-economic alternative to classical cross-coupling methods that rely on prefunctionalized reagents. Among them, atroposelective C–H carbonylation—including alkylation,⁶ alkenylation,⁷ and arylation⁸—has demonstrated remarkable advantages in enabling structural diversification with excellent stereocontrol (Scheme 1a). Despite these advances, atroposelective C–H allylation has been less explored and is largely limited to employment of olefins as allylating reagents.⁹ Although axially chiral allyl biaryls may serve as versatile synthetic intermediates enabling downstream diversifications, the inherent mechanistic complexity and the difficulty in balancing regio- and stereoselectivity make it challenging to develop a general and highly enantioselective strategy (Scheme 1a). Existing C–H bond allylation¹⁰ pathways typically proceed through: (1) outer-sphere trapping of metal allyl by an arene or by a chelation-assisted acidic alkyl C–H

group;¹¹ (2) alkene insertion– β -elimination sequences;^{9,12} or (3) allyl oxidative addition–reductive elimination (OA-RE) processes.¹³ The last involves a high-valent M-allyl intermediate with frequent alterations of the coordination sphere, leading to poor compatibility with C–H allylation and making it difficult to achieve precise stereocontrol (Scheme 1b). Indeed, this OA-RE pathway has been less explored due to compatibility challenges between C–H activation and metal-allyl formation. Nevertheless, this pathway is theoretically applicable to electron-poor arenes contingent on a proper selection of a low-valent metal catalyst.

Against this background, *gem*-difluorocyclopropanes¹⁴ (DFCs) have emerged as a unique allyl surrogate, providing an innovative and distinct approach to introduce a functionalized allyl fragment. Under transition-metal catalysis, their inherent ring strain drives C–C bond cleavage to generate a metal-allyl intermediate.¹⁵ Meanwhile, the strong electron-withdrawing nature of the fluorine substituents significantly modulates the electron density and leaving-group ability of this intermediate, enabling outer-sphere allylation with electron-rich arenes or olefins as in a Friedel-Crafts mechanism (Scheme 1b).¹⁶ The synergistic interplay between the strain-driven kinetic activation and the fluorine-induced electronic modulation provides opportunity for the sequential realization of C–H activation, allylic intermediate generation, and C–C coupling in a stereochemically controlled fashion within a single catalytic cycle (Scheme 1c), thus offering an operationally simple and potentially general solution to atroposelective C–H allylation. Nevertheless, only very few reports on asymmetric C–H bond allylation using DFCs have been disclosed.¹⁷

Herein, we report a Rh(I)-catalyzed stereoconvergent atroposelective C–H fluoroallylation using racemic *gem*-difluorocyclopropanes as bifunctional fluoroallyl precursors, providing an allyl framework with integrated fluorine atoms. This method efficiently constructs axially chiral biaryl

^a School of Chemistry and Chemical Engineering, Shaanxi Normal University, Xi'an 710062, China

^b Department of Chemistry, School of Science, Tianjin University, Tianjin, 300072, China

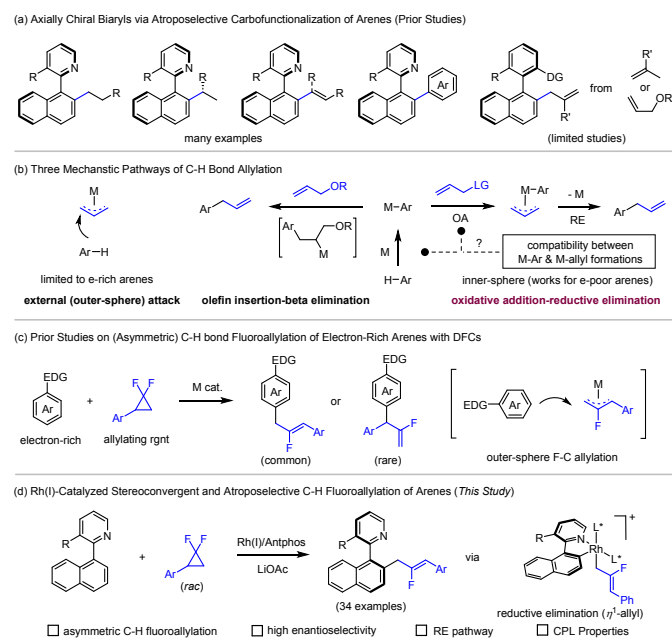
^c Frontiers Science Center for Flexible Electronics (FSCFE), Shaanxi Institute of Flexible Electronics (SIFE), Northwestern Polytechnical University (NPU), Xi'an 710072, China

^d State Key Laboratory of Chemistry and Utilization of Carbon-Based Energy Resources, College of Chemistry, Xinjiang University, Urumqi 830017, China



frameworks with excellent regio- and enantioselectivity. Within the Rh(I)/Rh(III) redox cycle, the η^1 -allyl-Rh(III) intermediate undergoes enantio-determining reductive elimination, achieving the first enantioselective installation of a fluoroallyl unit via atropselective C-H functionalization (Fig. 1c). The resulting products exhibit pronounced circularly polarized luminescence (CPL), highlighting their potential in high-performance chiral optoelectronic applications.

Scheme 1. C-H Bond Allylation of Arenes and Asymmetric Allylation via Reductive Elimination (RE).



Initial Optimization Studies. We began our investigation by screening chiral ligands using a Rh(I) catalyst in toluene in the presence of LiOAc (Figure 1). Bidentate P-N and P-P ligands (**L1**–**L5**) exhibited negligible activity for the coupling of arene **1a** with DFC **2a**, whereas a chiral dppp-type ligand (**L6**) afforded the desired product **3** with only moderate enantioselectivity. Monodentate phosphoramidites **L6** and **L7** displayed both low reactivity and poor enantioselectivity. Encouragingly, Antphos **L9** enabled the formation of **3** in excellent yield, albeit initially with modest reactivity. Notably, ortho substituents on the phenyl ring significantly influenced the reaction outcome, as exemplified by **L10**, which led to both poor reactivity and low enantioselectivity. Consequently, **L9** was chosen for further optimization studies.

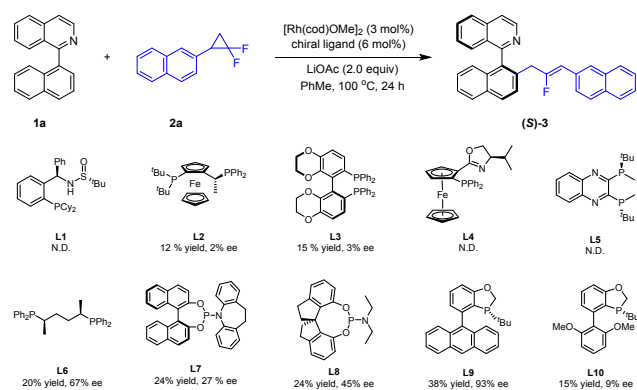


Figure 1. Reactions were carried out using 1-(naphthalen-1-yl)isoquinoline **1a** (0.1 mmol), **2a** (2.0 equiv), $[Rh(cod)OMe]_2$ (3

mol%), **L** (6 mol%) and LiOAc (2.0 equiv) in PhMe (2 mL) at 100 °C for 24 h under N_2 . Isolated yield. The ee was determined by HPLC analysis.

Subsequent optimization revealed that an alkali acetate additive was essential to maintain catalytic activity (Table 1 and the SI). When NaOAc was used as an additive, the choice of solvent exerted a significant impact on both reactivity and enantioselectivity, with toluene providing the best outcomes (entries 2-7). The employment of LiOAc and $AgBF_4$ (0.1 equiv) substantially enhanced the reaction efficiency (entry 8), while LiOAc still outperformed NaOAc in terms of both yield and selectivity (entry 9). Increasing the amount of $AgBF_4$ led to diminished reaction efficiency, likely due to undesired single-electron oxidation of the phosphine ligand. By contrast, other additives such as lithium carbonate or magnesium acetate, or the omission of LiOAc, completely suppressed the reaction.

Table 1. Optimization Studies of the Reaction Conditions.

entry	solvent	base	additive	ee (%)	yield (%)
1	DCE	NaOAc	--	--	0
2	PhMe	NaOAc	--	90	21
3	PhCl	NaOAc	--	70	24
4	PhCF ₃	NaOAc	--	50	28
5	EA	NaOAc	--	90	18
6	THF	NaOAc	--	76	15
7	PhMe	LiOAc	--	91	38
8	PhMe	LiOAc	$AgBF_4$	91	71
9	PhMe	NaOAc	$AgBF_4$	90	63
10	PhMe	--	$AgBF_4$	--	0
11	PhMe	Li_2CO_3	$AgBF_4$	--	<5
12	PhMe	$Mg(OAc)_2$	$AgBF_4$	--	<5

^aReactions were carried out using 1-(naphthalen-1-yl)isoquinoline **1a** (0.1 mmol), **2a** (2.0 equiv), $[Rh(cod)OMe]_2$ (3 mol%), **L9** (6 mol%) and $AgBF_4$ (10 mol%) in a solvent (2 mL) at 100 °C for 24 h under N_2 .

^bIsolated yield. ^cThe ee was determined by HPLC analysis.

RESULTS AND DISCUSSION

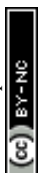
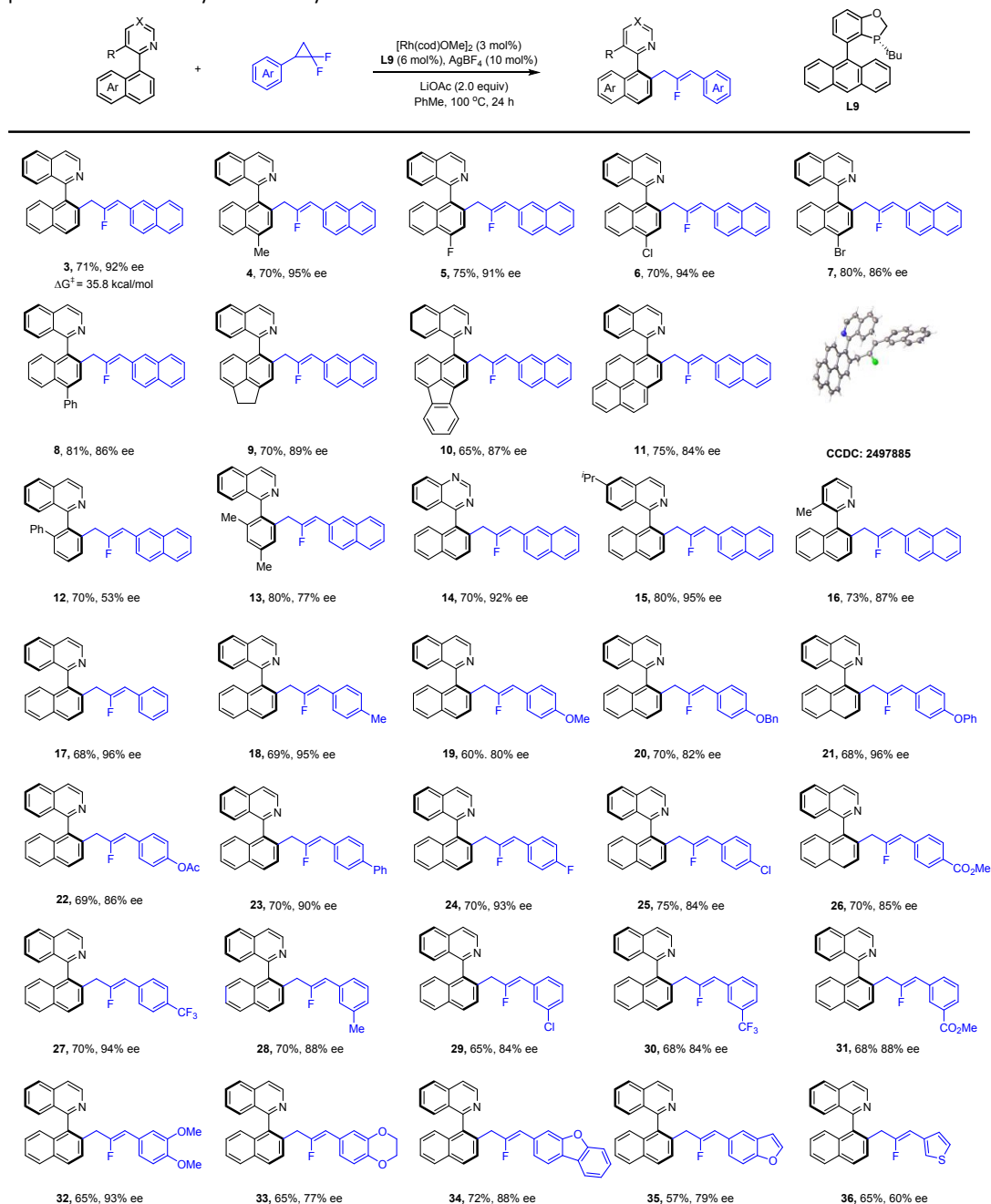
Substrate Scope. Having identified the optimal reaction conditions, we went on to investigate the generality of this catalytic system (Scheme 2). The scope of the heteroarene was investigated using **2a** as the coupling reagent. It was found that introduction of alkyl, halogen, and aryl group into the 4-position of the naphthalene ring had marginal impact on the efficiency and enantioselectivity of this coupling system (products **4**–**8**, 86–95% ee). The atropstability of product has been measured, and the large racemization barrier of 35.8 kcal/mol indicated its high configurational stability. Fusing a carbocycle into different positions of the naphthalene was also tolerated, and the enantioselectivity was only slightly affected (**9**–**11**, 84–89% ee). The absolute configuration of product **11** has been determined by X-ray crystallography (CCDC 2497885). In contrast, replacing the naphthalene ring with a (2-phenyl)phenyl group resulted in lower enantioselectivity (**12**, 53% ee). Further improved enantioselectivity was found when a 2,4-xyl group was used (**13**,



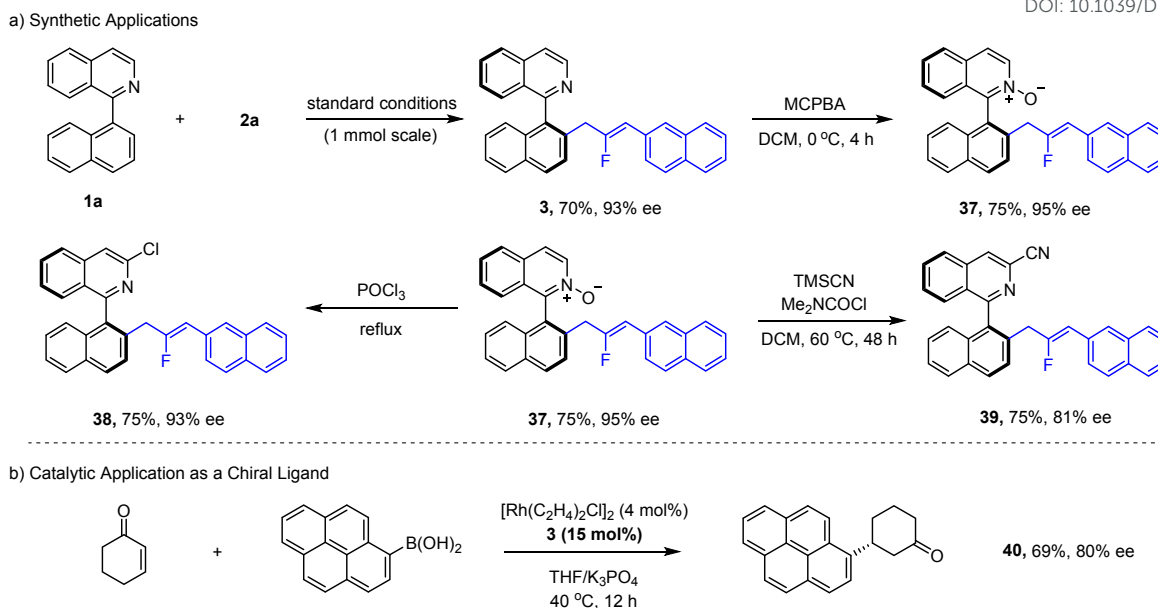
77% yield). The heterocyclic directing group was next investigated. The simple isoquinoline ring was smoothly extended to an alkyl-substituted one (**15**), a quinazoline (**14**), and an alkyl-pyridine (**16**). The aryl group in the DFC reagent was then briefly investigated. Simple para alkyl-, alkoxy-, phenoxy-, acetoxy-, aryl-, ester-, CF₃, and halogen-substituted phenyl group was well tolerated (**17-27**, 80-96% ee). A series of

electron-donating and -withdrawing meta groups (alkyl, sulfonyl, halogen, and ester) were also compatible (**28-32**, 84-96% ee). The aryl group was also switched to several heteroarene-fused aryls (**33-35**, 77-88% ee). In contrast, a 3-thienyl substituted DFC only reacted with moderate enantioselectivity (**36**). In all cases, the regioselectivity is excellent, and only the linear allylation product was observed.

Scheme 2. Scope of Substrates in Asymmetric Allylation.



Scheme 3. Synthetic and Catalytic Applications of a Selected Product.

View Article Online
DOI: 10.1039/D5SC08914J

Synthetic Applications. Synthetic transformations and catalytic applications were then investigated for a representative product (Scheme 3). The product **3** was prepared at a mmol scale, and no yield or enantioselectivity was compromised. *m*-CPBA oxidative of **3** occurred chemoselectively at the nitrogen site (**37**). Treatment of **37** with POCl₃ afforded a 3-chloroisoquinoline **38** in good yield. Deoxygenative cyanation proceeded smoothly to give **39** in good efficiency. In all cases, no erosion or only slight erosion of enantiopurity was observed. Moreover, product **37** also served as a chiral bidentate N-olefin ligand in Rh(I)-catalyzed Michael addition between an aryl boronic acid and cyclohexenone, affording chiral cyclohexanone **40** in good enantioselectivity.

Upon excitation (408 nm), strong fluorescence emission was observed with a maximum at 490 nm, and a quantum yield of 0.42 was measured (Figure 2a). Strong circular dichroism with mirror image was also observed for **10** and its enantiomer, indicating their chiral nature (Figure 2b). To our delight, prominent CPL was also observed for these two enantiomers (Figure 2c). Further analysis of the g_{lum} indicated that the luminescence dissymmetry factor is in the magnitude of 10⁻³ (Figure 2d). With these properties, this chiral product hold the potential for applications as an organic semiconductor or organic optical material.

Experimental Mechanistic Studies. A series of experiments have been conducted to explore the mechanism of this catalytic system (Scheme 4). H/D exchange studies were carried out to probe the sequence of C–H bond activation versus C–C activation (Scheme 4a). Noticeable H/D exchange between 1-aryloquinoline **1a** and D₂O was observed in the absence of a DFC reagent but in the presence of the Rh(I) catalysts and LiOAc (Scheme 4a). In contrast, no H/D exchange was detected when the LiOAc additive was omitted. In addition to the reversibility of C–H bond cleavage, these observations are consistent with the necessity of LiOAc in the catalytic reaction, and the reaction is likely initiated by C–H bond activation either via CMD mechanism or via C–H bond oxidative addition-reductive elimination of AcOH. To further probe this C–H activation event, KIE has been measured in parallel reactions (Scheme 4b). The KIE value of 2.1 suggests that the C–H cleavage probably occurs prior to the turnover-limiting step, and the barrier of C–H cleavage contributes to some extent to the overall barrier of the catalytic cycle. To probe the enantiocontrol event, the ratio of the **L9/Rh** was evaluated. It was found that ee of product **3** increases as the **L9/Rh** ratio increases, and the highest value (95–96% ee) was reached when the **L9/Rh** ratio was ≥ 2.5 (Scheme 4c). This observation seems to indicate reversible ligation of **L9** ligands,

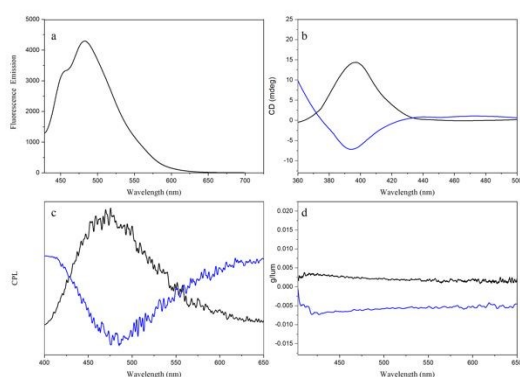


Figure 2. Photophysical Studies of Product 10 and its enantiomer (black line: product **10**, blue line: *ent*-**10**). (a) Fluorescence images ($E_m = 490$ nm, quantum yield = 0.42). (b) CD (circular dichroism) spectra of **10** and its enantiomer in THF (10⁻³ M) at room temperature. (c) CPL (circular polarized luminescence) spectra of **10** and the enantiomer in THF (10⁻³ M) at room temperature. (d) g_{lum} (luminescence dissymmetry factor) of **10** and its enantiomer.

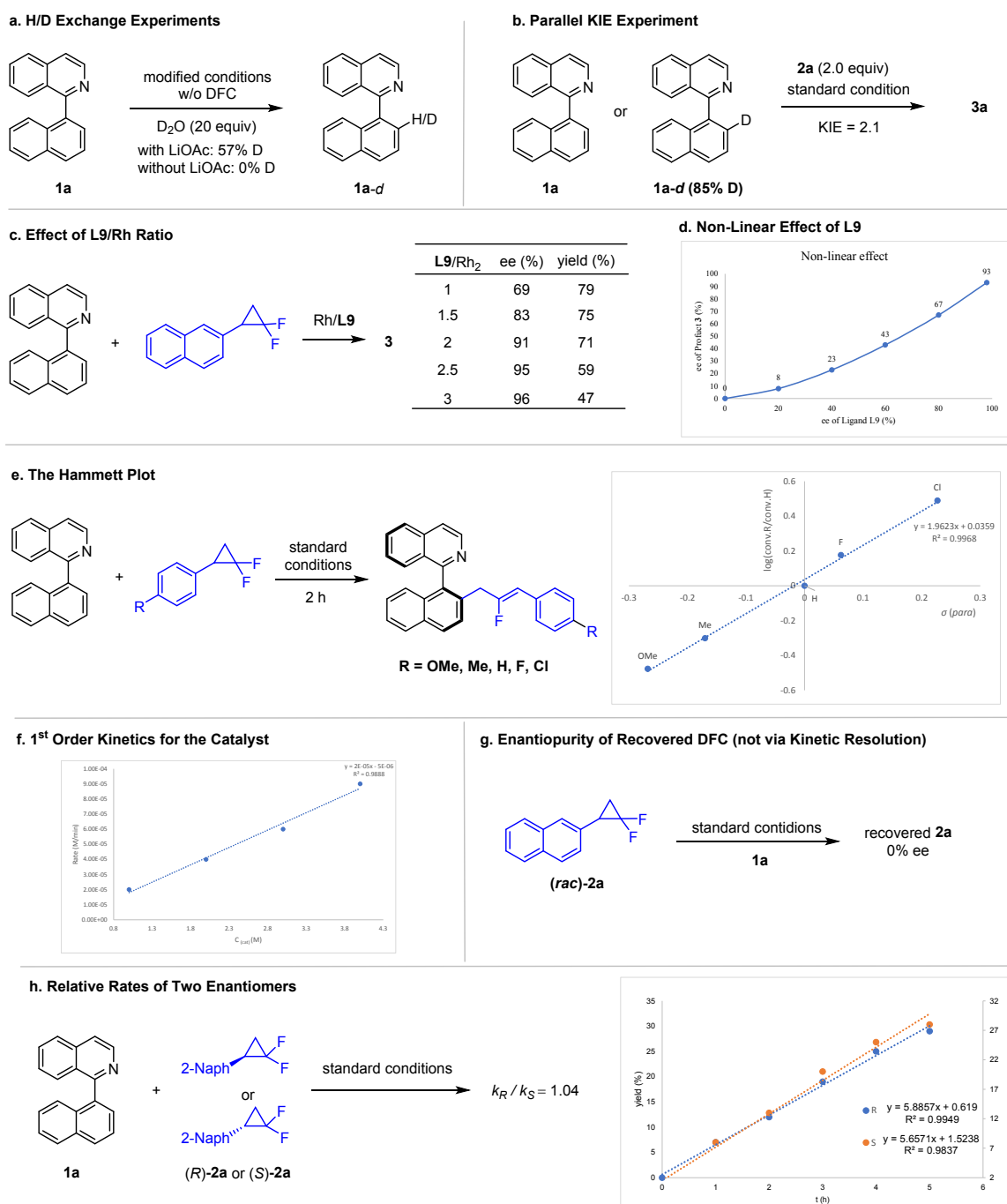
Besides the synthetic applications, the chiroptical properties of product **10** and its enantiomer were demonstrated (Figure 2).



which also agrees with our non-linear effect study, where a negative NLE was observed (Scheme 4d). Our kinetic studies also revealed 1st order dependence of the Rh(I) catalyst (Scheme 4f). Therefore, a monomeric rhodium with two monodentate **L9** ligands is likely operating during the EDS. To explore the electronic effect of the DFC reagent, linear free energy correlation has been performed (Scheme 4e). The rather large positive slope of $\rho = 2.0$ from the Hammett plot indicates that the C–C oxidative addition is likely

involved in the turnover-limiting step. Furthermore, only racemic **2a** was recovered from a catalytic reaction (Scheme 4g), suggesting that both enantiomers of **2a** reacted indiscriminably during the C–C oxidative addition. In line with this observation, both enantiomers of **2a** reacted with essentially the same rate in kinetic studies (Scheme 4h). Therefore, this enantioconvergent scenario stays contrast to the kinetic resolution pattern recently reported by Xia and coworkers.^{15d,17}

Scheme 4. Experimental Mechanistic Studies.



Computational Mechanistic Studies. Density functional theory (DFT) calculations were performed to gain deeper understanding of the reaction mechanism and the origin of the enantioselectivity (See Supporting Information and Figure 3). The reaction begins with C–H bond cleavage through the CMD process via transition state **TS3**, with an energy barrier of 21.3 kcal/mol relative to the reactant-coordinated intermediate **IM2** (Supporting Information). Subsequently, with the incoming *gem*-difluorocyclopropane **2**, the resulting intermediate **IM4** undergoes C–C oxidative addition via **TS4** to form the Rh(III) intermediate **IM5**. The subsequent β -F elimination proceeds through **TS5**, affording intermediate **IM6**. Anion exchange with the additive LiOAc and then with AgBF₄ generates cationic intermediate (S)-**IMO**. It should be noted that formation of LiF is likely a strong driving force. The computations show that **TS3** is lower in energy than **TS4**, indicating that the C–H bond cleavage step is reversible, which is consistent with the experimental observations (Scheme 4a).

Accordingly, the energy profile of the full catalytic cycle can be divided into two regions: (i) prior to the C–C reductive elimination and (ii) the C–C reductive elimination step. Therefore, the energies associated with the C–C reductive elimination were calculated relative to intermediate (S)-**IMO** and are presented in Figure 3 (the key reductive elimination step is depicted in Figure 3, with the results of the other steps included in the Supporting Information). Both bisligated and monoligated reaction pathways were considered. The computations indicate that the two pathways exhibit nearly identical activation barriers and enantioselectivities, implying that both pathways are likely accessible under the reaction conditions. It should be mentioned that the interconversion of the key rhodacyclic Rh(I) aryl intermediates (S)-**IMO** and (R)-**IMO** via transition state **TS2** is kinetically feasible, confirming that the C–C reductive elimination is the enantioselectivity-determining step of the reaction. Furthermore, the C–C reductive elimination step has the highest energy barrier among all steps, which thus represents the rate-determining step of the reaction. Furthermore, the C–C reductive elimination step has the highest energy barrier among all steps, which thus represents the rate-determining step of the reaction.

The calculations indicate that in the bisligated reaction pathway, the transition state (S)-**TS1** is 3.0 kcal/mol lower in energy than (R)-**TS1**, which corresponds to a predicted ratio of 98:2 at the reaction temperature, consistent with the experimentally observed enantioselectivity of 96% ee. Scrutiny of the optimized structures reveals that the enantioselectivity mainly arises from a stabilizing π - π interaction between the reacting arene **1a** moiety and ligand **L9** in (S)-**TS1**, which is absent in (R)-**TS1**, rendering the (S)-**TS1** energetically more favorable. On the other hand, in the monoligated reaction pathway, **L9** acts as a bidentate mode in both (S)-**TS1'** and (R)-**TS1'**, with the aryl ring of **L9** engaging in coordination interactions with the Pd center. The transition state (S)-**TS1'** is 3.2 kcal/mol lower in energy than (R)-**TS1'**, primarily because the stabilizing interaction in (S)-**TS1'** is stronger than that in (R)-**TS1'**.

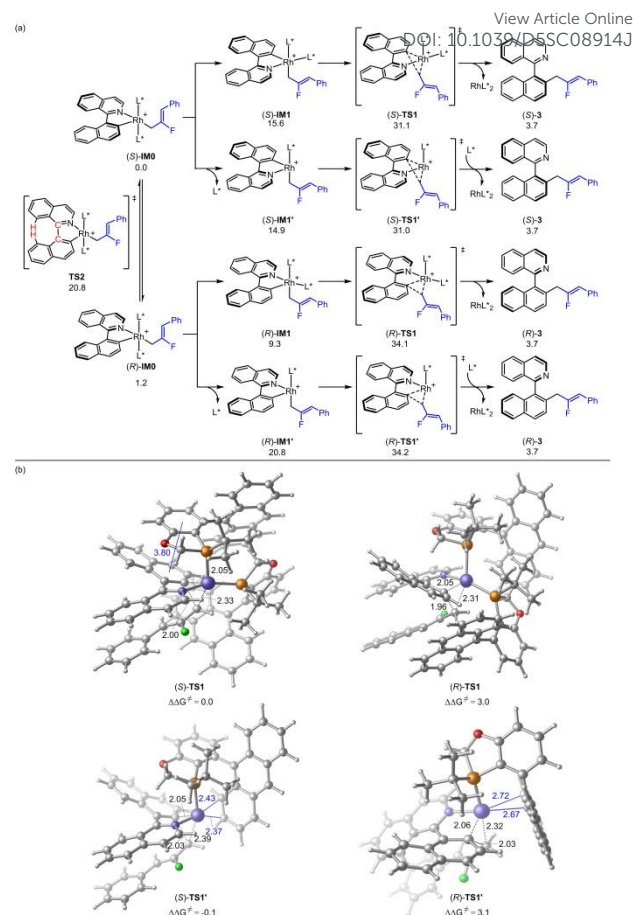


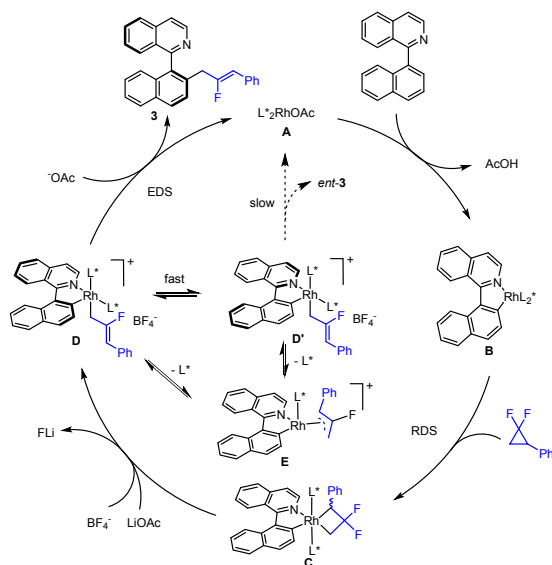
Figure 3. DFT study on C–C reductive elimination ($L^* = \mathbf{L9}$). Energies and bond distances are given in kcal/mol and Å, respectively.

A Plausible mechanism for this catalytic system is proposed (Scheme 5). Starting from a Rh(I) acetate bearing electron-rich chiral phosphine ligands (**A**), C–H bond oxidative addition and subsequent elimination of AcOH gives a rhodacyclic Rh(I) aryl intermediate (**B**). The alternative mechanism of acetate-assisted C–H activation cannot be ruled out at the current stage. Subsequently, indiscernible C–C bond oxidative addition of racemic DFC takes place to generate a four-membered Rh(III) intermediate (**C**), which then undergoes β -F elimination to give a cationic Rh(III) allyl species (**D**). It is proposed that fluoride abstraction by LiOAc plays an important role in ensuring the catalytic activity, driven by formation of insoluble LiF. The resulting Rh(III) allyl is proposed to undergo rapid epimerization of the chiral axis (**D** and **D'**),¹⁸ and the intermediate **D** undergoes more rapid C–C reductive elimination, producing product **3** together with the Rh(I) for the next cycle. Based on our mechanistic studies, while the Rh(III) allyl monophosphine intermediate (**E**) may also reductively eliminates, the enantioselectivity of the product is lower from this manifold. In the catalytic system, the AgBF₄ possibly participates in anion exchange with the acetate to give a cationic five-coordinate intermediate **D**, priming subsequent C–C reductive elimination. In anion exchange with the acetate to give a cationic



five-coordinate intermediated **D**, priming subsequent C-C reductive elimination.

Scheme 5. Proposed Catalytic Cycle.



CONCLUSIONS

In summary, we have developed a Rh(I)-catalyzed stereoconvergent C-H fluoroallylation of non-electron-rich arenes in the presence of a chiral monodentate ligand for the efficient construction of axially chiral biaryls. Utilizing racemic gem-difluorocyclopropanes as bifunctional precursors, the reaction proceeds via a Rh(I)/Rh(III) oxidative addition–reductive elimination cycle, enabling C–H activation, β -F elimination, and rapid epimerization of the chiral axis in an intermediate to achieve excellent regio- and enantioselectivity. The LiOAc additive plays a key role as a fluoride scavenger as well as a base to facilitate the C–H activation. DFT calculations elucidate the key factors governing stereocontrol, highlighting the precise synergy between C–H activation and allyl introduction. The resulting biaryls were accessed in high regio- and enantioselectivity and display pronounced circularly polarized luminescence (CPL), suggesting their promise as functional components in high-performance chiral optoelectronic materials.

Data Availability

Further details of the experimental procedure, ^1H and ^{13}C NMR, HPLC spectra, and X-ray crystallographic data are available in the ESI.

Author Contributions

X.L. and F.W. conceived and directed the project. J.L. and F.W. performed the experimental studies. X.H. performed DFT studies under the guidance of G.H. F.W., Z.-Q. R., and X.L. wrote the manuscript.

Conflicts of Interest

The authors declare no competing financial interests.

Article Online
DOI: 10.1039/D5SC08914J

ACKNOWLEDGMENT

Financial support from the National Natural Science Foundation of China (No. 22371175 and 22471191) and research fund from the Shaanxi Normal University are gratefully acknowledged.

Notes and References

- (a) J. Chang, J. Reiner and J. Xie, *Chem. Rev.*, 2005, **105**, 4581–4609; (b) K. Ding, H. Guo, X. Li, Y. Yuan and Y. Wang, *Top. Catal.*, 2005, **35**, 105–116; (c) Y.-M. Li, F.-Y. Kwong, W.-Y. Yu and A. S. C. Chan, *Coord. Chem. Rev.*, 2007, **251**, 2119–2144; (d) M. P. Carroll and P. J. Guiry, *Chem. Soc. Rev.*, 2014, **43**, 819–833; (e) H. Zhang and F. Shi, *Acc. Chem. Res.*, 2022, **55**, 2562–2580; (f) H. Zhang, T. Li, S. Liu and F. Shi, *Angew. Chem. Int. Ed.*, 2024, **63**, e202311053; (g) A. Gaucherand, E. Yen-Pon, A. Domain, A. Bourhis, J. Rodriguez and D. Bonne, *Chem. Soc. Rev.*, 2024, **53**, 11165–11206.
- (a) J. Clayden, W. J. Moran, P. J. Edwards and S. R. LaPlante, *Angew. Chem. Int. Ed.*, 2009, **48**, 6398–6401, (b) S. R. LaPlante, L. D. Fader, K. R. Fandrick, D. R. Fandrick, O. Hucke, R. Kemper, S. P. F. Miller and P. J. Edwards, *J. Med. Chem.* 2011, **54**, 7005–7022, (c) A. Zask, J. Murphy and G. A. Ellestad, *Chirality*, 2013, **25**, 265–274, (d) S. T. Toenjes and J. L. Gustafson, *Future Med. Chem.*, 2018, **10**, 409–422, (e) M. Basilaia, M. H. Chen, J. Secka and J. L. Gustafson, *Acc. Chem. Res.*, 2022, **55**, 2904–2919, (f) S. Perreault, J. Chandrasekhar and Patel, *L. Acc. Chem. Res.*, 2022, **55**, 2581–2593.
- (a) J. Chen and Y. Cao, *Rapid Commun.*, 2007, **28**, 1714–1742, (b) Q. Li, L. Green, N. Venkataraman, I. Shiyonovskaya, A. Khan, A. Urbas and J. W. Doane, *J. Am. Chem. Soc.*, 2007, **129**, 12908–12909, (c) Pu, L. *Acc. Chem. Res.*, 2012, **45**, 150–163, (d) K. Takaishi, M. Yasui and T. Ema, *J. Am. Chem. Soc.*, 2018, **140**, 5334–5338, (e) D. Zhang, M. Li and C. Chen, *Chem. Soc. Rev.* 2020, **49**, 1331–1343.
- (a) E. Kumarasamy, R. Raghunathan, M. P. Sibi and J. Sivaguru, *Chem. Rev.*, 2015, **115**, 11239–11300, (b) B. Zilite, A. Castrogiovanni, C. Sparr, *ACS Catal.*, 2018, **8**, 2981–2988, (c) A. Link and C. Sparr, *Stereoselective Arene Formation. Chem. Soc. Rev.* 2018, **47**, 3804–3815, (d) J. K. Cheng, S. Xiang, S. Li, L. Ye and B. Tan, *Chem. Rev.*, 2021, **121**, 4805–4902, (e) G. Mei, W. L. Koay, C. Guan and Y. Lu, *Chem*, 2022, **8**, 1855–1893, (f) W. Qin, Y. Liu and H. Yan, *Acc. Chem. Res.* 2022, **55**, 2780–2795, (g) J. Feng, L. Xi, C. Lu and R.-R. Liu, *Chem. Soc. Rev.*, 2024, **53**, 9560–9581, (h) S. Xiang, W. Ding, Y. Wang and B. Tan, *Nat. Catal.*, 2024, **7**, 483–498.
- For selected reviews, see: (a) G. Liao, T. Zhou, Q. Yao and B. F. Shi, *Chem. Commun.*, 2019, **55**, 8514–8523, (b) M. I. Lapuh, S. Mazeh and T. Besset, *ACS Catal.*, 2020, **10**, 12898–12919, (c) C.-X. Liu, W. Zhang, S. Yin, Q. Gu, and S.-L. You, *J. Am. Chem. Soc.* 2021, **143**, 14025–14040, (d) P. Qian, T. Zhou and B. F. Shi, *Chem. Commun.*, 2023, **59**, 12669–12684, (e) C.-X. Liu, S.-Y. Yin, F. Zhao, H. Yang, Z.



- Feng, Q. Gu and S.-L. You, *Chem. Rev.* 2023, **123**, 10079–10134, (f) S. Choppin and J. Wencel-Delor, *Acc. Chem. Res.*, 2023, **56**, 189–202, (g) G. Liao and B.-F. Shi, *Acc. Chem. Res.* 2025, **58**, 1562–1579.
- (a) F. Kakiuchi, P. Le Gendre, A. Yamada, H. Ohtaki and S. Murai, *Tetrahedron Asymmetry*, 2000, **11**, 2647–2651, (b) M. Xiong, Z. Yan, S. Chen, J. Tang, Y. Fan, D Xing, *ACS Catal.* 2024, **14**, 7243–7255, (c) F. Li, Y. Luo, J. Ren, Q. Yuan, D. Yan and W. B. Zhang, *Org. Lett.* 2024, **26**, 6835–6840.
 - (a) J. Zheng and S.-L. You, *Angew. Chem. Int. Ed.*, 2014, **53**, 13244–13247, (b) J. Zheng, W. Cui, C. Zheng and S.-L. You, *J. Am. Chem. Soc.*, 2016, **138**, 5242–5245, (c) S. X. Li, Y. N. Ma and S. D. Yang, *Org. Lett.*, 2017, **19**, 1842–1845, (d) J. Luo, T. Zhang, L. Wang, G. Liao, Q.-J. Yao, Y.-J. Wu, B. Zhan, Y. Lan, X. Lin and B.-F. Shi, *Angew. Chem. Int. Ed.*, 2019, **58**, 6708–6712, (e) B. Zhan, L. Wang, J. Luo, X. Lin, and B. F. Shi, *Angew. Chem. Int. Ed.*, 2020, **59**, 3568–3572, (f) P. Vázquez-Domínguez, A. Romero Arenas, R. Fernández, J. M. Lassaletta and A. Ros, *ACS Catal.*, 2023, **13**, 42–48, (g) Q. Zhou, S.-Y. Yin, D. Zheng, W. Zhang, S. Zhang, Q. Gu, and S.-L. You, *Synlett*, 2023, **34**, 1442–1446.8
 - (a) A. Ros, B. Estepa, P. Ramírez-López, E. Á lvarez, R. Fernández and J. M. Lassaletta, *J. Am. Chem. Soc.* 2013, **135**, 15730–15733, (b) Q. Wang, Z. Cai, C. Liu, Q. Gu and S.-L. You, *J. Am. Chem. Soc.*, 2019, **141**, 9504–9510, (c) M. Tian, D. Bai, G. Zheng, J. Chang and X. Li, *J. Am. Chem. Soc.*, 2019, **141**, 9527–9532, (d) Q. Wang, W. Zhang, H. Song, J. Wang, C. Zheng, Q. Gu and S.-L. You, *J. Am. Chem. Soc.*, 2020, **142**, 15678–15685, (e) Q. Nguyen, S. Guo, T. Royal, O. Baudoin, *J. Am. Chem. Soc.*, 2020, **142**, 2161–2167, (f) Q. Wang, W. Zhang, C. Zheng, Q. Gu and S.-L. You, *J. Am. Chem. Soc.*, 2021, **143**, 114–120.
 - (a) G. Liao, H. Chen, Q. Yao, Y. Xia, J. Luo and B.-F. Shi, *Angew. Chem. Int. Ed.*, 2018, **57**, 17151–17155, (b) G. Liao, T. Zhang, L. Jin, B. Wang, C. Xu, Y. Lan, Y. Zhao and B.-F. Shi, *Angew. Chem. Int. Ed.*, 2022, **61**, e202115221.
 - Reviews on C-H bond allylation: (a) N. K. Mishra, S. Sharma, J. Park, S. Han, I. S Kim, *Chem*, 2021, **7**, 555–605.
 - Asymmetric allylation of acidic C-H sites: (a) L. Fan, S. Luo, S. Chen, T. Wang and P. Wang and L. Gong, *Angew. Chem. Int. Ed.*, 2019, **58**, 16806–16810, (b) T. Wang, L. Zhu, S. Luo, Z. Nong, P. Wang and L. Gong, *J. Am. Chem. Soc.*, 2021, **143**, 20454–20461, (c) Z. Nong, L. Zhu, T. Wang, L. Fan, P. Wang, L. Gong, *Nat. Synth.*, 2022, **1**, 487–496, Allylation of electron-rich arenes: (d) C.-X. Zhuo and S.-L. You, *Acc. Chem. Res.*, 2014, **47**, 2558–2573, (e) B. M. Trost and M. U. Frederiksen, *Angew. Chem. Int. Ed.*, 2005, **44**, 308–310.
 - Allylation via olefin insertion and β -H elimination: (a) J. Kwak, Y. Ohk, Y. Jung and S. Chang, *J. Am. Chem. Soc.*, 2012, **134**, 17778–17788, (b) S. Wang and N. Cramer, *Angew. Chem. Int. Ed.*, 2019, **58**, 2514–2518. Allylation via insertion- β -O elimination (c) R. Mi, G. Zheng, Z. Qi and X. Li, *Angew. Chem. Int. Ed.*, 2019, **58**, 17666–17670, (d) X. Yang, G. Zheng and X. Li, *Angew. Chem. Int. Ed.*, 2019, **58**, 322–326, (e) K. Ozols, S. Onodera, Ł. Wozniak and Nicolai Cramer. *Angew. Chem. Int. Ed.*, 2021, **60**, 655–659, (f) Y. Zheng, W. Zhang, Q. Gu, C. Zheng and S.-L. You, *Nat. Commun.*, 2023, **14**, 1094.
 - (a) S. Fan, F. Chen and X. Zhang, *Angew. Chem. Int. Ed.*, 2011, **50**, 5918–5923, (b) S. Y. Lee and J. F. Hartwig, *J. Am. Chem. Soc.*, 2016, **138**, 15278–15284, (c) W. Xie, and S. Chang, *Angew. Chem. Int. Ed.*, 2016, **55**, 1876–1880, (d) K. Liu, T. Li, D. Liu, W. Li, J. Han, C. Zhu and J. Xie, *Sci. China Chem.*, 2021, **64**, 1959–1963.
 - (a) Fedoryn'ski. M, *Chem. Rev.* 2003, 103, 1099–1132, (b) F. Wang, T. Luo, J. Hu, Y. Wang, H. S. Krishnan, P. V. Jog, S. K. Ganesh, G. K. S. Prakash and G. A. Olah, *Angew. Chem. Int. Ed.*, 2011, **50**, 7153–7157, (c) W. R. Dolbier and M. A. Battiste, *Chem. Rev.*, 2003, **103**, 1071–1098, (d) Y. Zeng, Z.-T. Jiang and Y. Xia, *Chem Commun.*, 2024, **60**, 3764–3773.
 - (a) E.-A. M. Ahmed, A. M. Y. Suliman, T. Gong, Y. Fu, *Org. Lett.*, 2019, **21**, 5645–5649, (b) Y. Zeng, H. Yang, J. Du, Q. Huang, G. Huang and Y. Xia, *Chem. Sci.* 2022, **13**, 12419–12425, (c) Y. Ai, H. Yang, C. Duan, X. Li and S. Yu, *Org. Lett.*, 2022, **24**, 5051–5055, (d) Z. Jiang, Z. Chen, Y. Zeng, J. Shi, Y. Xia, *Org. Lett.*, 2022, **24**, 6176–6181, (e) J. Sun, H. Ye, F. Sun, Y. Pan, X. Zhu, X. Wu, (f) H. Qian, H. D. Nguyen, L. Lv, S. Chen and Z. Li, *Angew. Chem. Int. Ed.*, 2023, **62**, e202303271.
 - (a) Z. Jiang, J. Huang, Y. Zeng, F. Hu and Y. Xia, *Angew. Chem. Int. Ed.*, 2021, **60**, 10626–10631, (b) Z. Fu, J. Zhu, S. Guo, A. Lin, *Chem. Commun.*, 2021, **57**, 1262–1265, (c) Z. Jiang, Y. Zeng and Y. Xia, *Synlett*, 2021, **32**, 1675–1682, (d) X. Wu, Y. Zeng, Z. Jiang, Y. Zhu, L. Xie and Y. Xia, *Org. Lett.*, 2022, **24**, 8429–8434, (e) X. Wu, X. Song, and Y. Xia, *Adv. Sci.*, 2024, **11**, 2401243, (f) Y. Zeng, H. Gao, Z. Jiang, Y. Zhu, J. Chen, H. Zhang, G. Lu and Y. Xia, *Nat. Commun.*, 2024, **15**, 4317.
 - (a) H. Yang, Y. Zeng, X. Song, L. Che, Z. Jiang, G. Lu, Y. Xia, *Angew. Chem. Int. Ed.*, 2024, **63**, e202403602, (b) Z. Su, B. Tan, H. He, K. Chen, S. Chen, H. Lei, T. Chen, S. Ni and Z. Li, *Angew. Chem. Int. Ed.*, 2024, **63**, e202402038, (c) Z. Yang, Y. Gong, Q. Gu and S.-L. You, *ACS Catal.*, 2025, **15**, 4287–4293.
 - (a) J. A. Carmona, V. Hornillos, P. Ramírez-López, A. Ros, J. Iglesias-Sigüenza, E. Gómez-Bengoa, R. Fernández and J. M. Lassaletta, *J. Am. Chem. Soc.*, 2018, **140**, 11067–11075, (b) A. Romero-Arenas, V. Hornillos, J. Iglesias-Sigüenza, R. Fernández, J. López-Serran, A. Ros and J. M. Lassaletta, *J. Am. Chem. Soc.*, 2020, **142**, 2628–2639.



Data Availability

Further details of the experimental procedure, ^1H and ^{13}C NMR, HPLC spectra, and X-ray crystallographic data are available in the ESI.

